chemosensors

MDPI

Article

Electrochemical Biosensor Based on Chitosan- and Thioctic-Acid-Modified Nanoporous Gold Co-Immobilization Enzyme for Glycerol Determination

Caiyun Yan [1], Kaifeng Jin [2], Xiangyi Luo [3], Jinhua Piao [1,*] and Fang Wang [4,*]

[1] School of Food Science and Engineering, South China University of Technology, Guangzhou 510641, China; 201920124942@mail.scut.edu.cn
[2] School of Life Science, Jilin University, Changchun 130012, China; jinkf1620@mails.jlu.edu.cn
[3] Department of Mathematics, Northeast Forestry University, Harbin 150040, China; luoxiangyi@nefu.edu.cn
[4] School of Environmental Engineering and Chemistry, Luoyang Institute of Science and Technology, Luoyang 471023, China
* Correspondence: jhpiao@scut.edu.cn (J.P.); wangfang1116@163.com (F.W.)

Abstract: An electrochemical biosensor based on chitosan- and thioctic-acid-modified nanoporous gold (NPG) co-immobilization glycerol kinase (GK) and glycerol-3-phosphate oxidase (GPO) was constructed for glycerol determination in wine. The NPG, with the properties of porous microstructure, large specific surface area, and high conductivity, was beneficial for protecting the enzyme from inactivation and denaturation and enhancing electron transfer in the modified electrode. The co-immobilization of the enzyme by chitosan-embedding and thioctic-acid-modified NPG covalent bonding was beneficial for improving the catalytic performance and stability of the enzyme-modified electrode. Ferrocene methanol (Fm) was used as a redox mediator to accelerate the electron transfer rate of the enzyme-modified electrode. The fabricated biosensor exhibited a wide determination range of 0.1–5 mM, low determination limit of 77.08 μM, and high sensitivity of 9.17 μA mM^{-1}. Furthermore, it possessed good selectivity, repeatability, and stability, and could be used for the determination of glycerol in real wine samples. This work provides a simple and novel method for the construction of biosensors, which may be helpful to the application of enzymatic biosensors in different determination scenarios.

Keywords: electrochemical biosensor; glycerol; nanoporous gold; glycerol kinase; glycerol-3-phosphate oxidase

Citation: Yan, C.; Jin, K.; Luo, X.; Piao, J.; Wang, F. Electrochemical Biosensor Based on Chitosan- and Thioctic-Acid-Modified Nanoporous Gold Co-Immobilization Enzyme for Glycerol Determination. *Chemosensors* **2022**, *10*, 258. https://doi.org/10.3390/chemosensors10070258

Academic Editor: Boris Lakard

Received: 31 May 2022
Accepted: 29 June 2022
Published: 2 July 2022

1. Introduction

Glycerol, also known as 1,2,3-propanetriol, is a nontoxic, colorless, odorless, sweet, hygroscopic and thick liquid. As the main byproduct of the *Saccharomyces cerevisae* fermentation process, glycerol naturally exists in various fruit drinks, wine, beer, honey, etc. [1]. Due to its sweetness and viscosity, a certain amount of glycerol can weaken the bitter odor and make the wine taste round; the glycerol content is an important indicator for evaluating the quality of wine [2,3]. The final concentration of glycerol generated in wine fermentation is approximately a 1:10 ratio of the ethanol formed, which is in the range of 1 to 10 g L^{-1} [1,4]. Deviations from this value might indicate deterioration of raw materials, technological alterations of wine production, or even adulteration by adding exogenous glycerol [5]. Therefore, developing a rapid, sensitive, economical, and reliable determination method for the routine analysis of glycerol concentration is significant for protecting the health and safety of consumers.

Various analytical methods for the detection and quantification of glycerol have been proposed, which include gas chromatography [6], liquid chromatography [7], spectrophotometric [8] and enzymatic methods [9], etc. Unfortunately, most of the conventional methods

have the disadvantage of high cost, time-consuming, tedious pre-treatment as well as the need for trained personnel [9,10]. Electrochemical methods are preferred owing to their reusability, rapidity, sensitivity, and accuracy [11]. Notably, the electrochemical enzyme biosensor has become the most preferred candidate for glycerol determination owing to its superior catalytic activity, rapid response, and high selectivity [1,12]. For example, Narwal et al. fabricated a glycerol biosensor based on co-immobilization of glycerol kinase (GK) and glycerol-3-phosphate oxidase (GPO) nanoparticles onto a pencil graphite electrode. The biosensor showed a wide linearity range for glycerol determination, from 0.01 to 45 mM, with a determination limit of 0.0001 µM [12]. However, some adverse factors, such as the electron transfer obstruction caused by enzyme proteins, the inactivation of enzyme molecules, the instability of the enzyme-modified electrode, etc., still exist and affect the performance of the enzymatic biosensor, which limits its application [13]. Therefore, improving the performance of the enzyme electrode by modification is necessary.

To overcome the shortcomings mentioned above of the biosensor, nano materials with high specific surface area and good conductivity, e.g., carbon nanomaterials [14–16], metal and metal oxide nanoparticles [17,18], etc., are used as modification materials to immobilize the enzyme, so as to improve the catalytic efficiency and stability of the biosensor [14–17]. Three-dimensional nanoporous gold (NPG) receives attention as an electrochemical sensor because of its large surface area, high conductivity, and good electrocatalytic activity [18,19]. The notable biocompatibility of NPG makes it an attractive support platform for the immobilization of enzymes. For example, Yang et al. constructed a type of lipase-NPG biocomposite by the covalent coupling method, which could retain over 85% of its initial catalytic activity after ten recycles and exhibit great resistance to denaturation over a broader range of pH values and temperatures [20]. NPG can be prepared by dealloying [21,22], anodizing [23], and template synthesis [24]. However, these methods generally suffer from high energy consumption, impurity pollution, and being environmentally unfriendly. Thus, the Dynamic Hydrogen Bubble Template (DHBT) method, relying on the generated hydrogen bubbles as dynamic templates without the need of any removal of additional organic or inorganic templates, is a great choice for the fabrication of porous micro/nano structures [25,26].

Thioctic acid (TA), a disulfide with a terminal -COOH group, is used for enzyme immobilization onto NPG by covalent binding [27]. It can form stable self-assembled monolayer (SAM) on a gold surface with two S-Au bonds conveniently, while the terminal groups are able to covalently bind with other molecules. Additionally, chitosan (CHIT), with great film-forming ability and adhesion, is encapsulated to further prevent enzymes from falling off [28].

Accordingly, a novel ultrasensitive, rapid, and stable electrochemical biosensor was developed for glycerol determination in this work. In this biosensor, three-dimensional nanoporous gold was prepared by the Dynamic Hydrogen Bubble Template method and used as a carrier for the enzyme. Glycerol kinase (GK) and glycerol-3-phosphate oxidase (GPO) were used as biorecognition elements, TA as a bifunctional building block, CHIT as a binder, and ferrocene methanol (Fm) with favorable redox reversibility as a redox mediator. Figure 1 shows the construction process of the GK/GPO/CHIT/TA/NPG/AuE glycerol biosensor, and the catalytic reaction process of glycerol on the enzyme-modified electrode may be followed the equations:

$$\text{Glycerol} + \text{ATP} \xrightarrow{\text{GK/Mg}^{2+}} \text{G3P} + \text{ADP} \quad (1)$$

$$\text{G3P} + \text{GPO(FAD)} \rightarrow \text{DHAP} + \text{GPO(FADH}_2\text{)} \quad (2)$$

$$2\text{Fm}^+ + \text{GPO(FADH}_2\text{)} \rightarrow 2\text{Fm} + \text{GPO(FAD)} + 2\text{H}^+ \quad (3)$$

$$2\text{Fm} \rightarrow 2\text{Fm}^+ + 2\text{e}^- \quad (4)$$

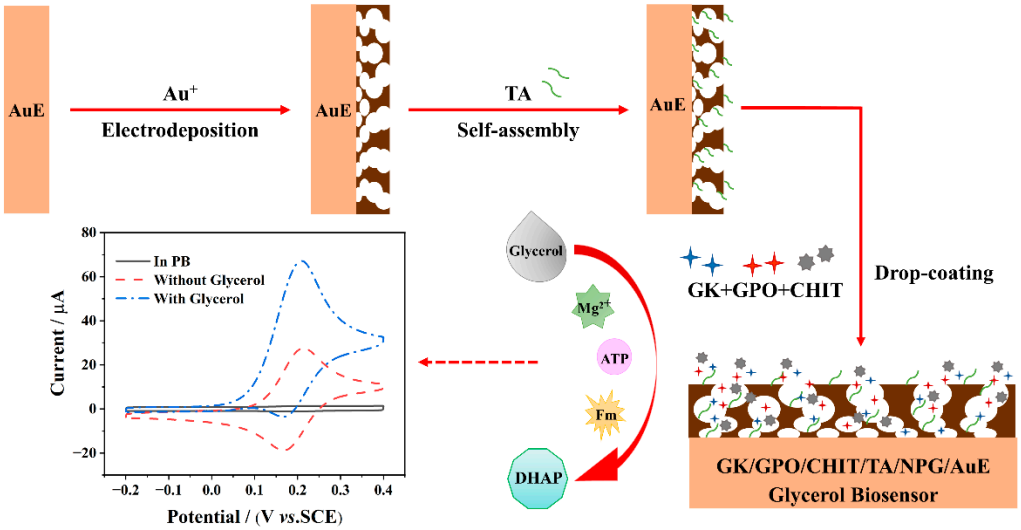

Figure 1. Schematic illustration of the construction process of the GK/GPO/CHIT/TA/NPG/AuE glycerol biosensor.

Firstly, glycerol can be phosphorylated to glycerol 3-phosphate (G3P) in the presence of Glycerol kinase, adenosine triphosphate (ATP), and $MgCl_2$. Then, G3P is oxidized to dihydroxyacetone phosphate (DHAP) while the active center of glycerol-3-phosphate oxidase, flavin adenine dinucleotide (FAD), is reduced to $FADH_2$ [29]. Fm^+ is reduced to Fm during the oxidation process of the $FADH_2$ [13]. The developed biosensor possesses excellent sensitivity, selectivity, and stability and good applicability for glycerol determination in real samples. This work provides a promising tool for the rapid determination of some biomolecules in different application scenarios.

2. Materials and Methods

2.1. Materials and Chemicals

Glycerol kinase (GK, 37.5 U mg^{-1}), glycerol-3-phosphate oxidase (GPO, 74.5 U mg^{-1}), chitosan (CHIT, average molecular weight 200 kDa, deacetylation degree $\geq$ 90%), ferrocene methanol (Fm, 98%), 1-ethyl-3-[3-dimethylaminopropyl]-carbodiimide hydrochloride (EDC, 99%), and N-hydroxy-succinimide (NHS, 99%) were purchased from Shanghai Yuanye Bio-Technology Co., Ltd. (Shanghai, China). Hydrogen tetrachloroaurate (III) xhydrate ($HAuCl_4$ H_2O, 99.9%) was obtained from Bide Pharmatech Ltd. (Shanghai, China). DL-Thioctic acid (TA, 99%) was provided by Shanghai Macklin Biochemical Co., Ltd. (Shanghai, China). Glycerol (99.0%) came from Damao Chemical reagent factory (Tianjin, China). The red and white wines were purchased from China Great Wall Wine Co., Ltd. (Beijing, China). The 0.1 M phosphate buffer (PB) with different pH values was prepared by mixing 0.1 M NaH_2PO_4 and 0.1 M Na_2HPO_4 solutions in different volume ratios. All chemicals and regents were of analytical grade and used without any further purification.

2.2. Instruments

The microstructure and morphology of the prepared materials were characterized by scanning electron microscopy (SEM, Zeiss Supra40, Bayreuth, Germany). Chemical compositions were measured using an X-MaxN20 energy dispersive X-ray spectrometer (EDS, Oxford, UK). Electrochemical measurements were carried out by a three-electrode system on a CHI 660E Electrochemical Workstation (Shanghai Chenhua Instrument Co., Ltd., Shanghai, China). The as-prepared modified electrode, platinum sheet, and saturated calomel electrode (SCE) were used as a working electrode, auxiliary electrode, and reference electrode, respectively. The electrochemical performances were measured by cyclic voltammetry (CV) and electro-chemical impedance spectroscopy (EIS). EIS measurements

were performed in the frequency range of 0.1 Hz to 100 kHz. All the experiments were carried out at ambient temperature.

2.3. Preparation of NPG/AuE-Modified Electrode

The bare gold electrode (AuE, 3 mm diameter) was polished with alumina powders (0.05 μm), rinsed with ethanol and distilled water in an ultrasonic bath, respectively, and then electrochemically cleaned in 1 M H_2SO_4 solution from −0.1 to 1.5 V at a scan rate of 100 $mV \cdot s^{-1}$ until reproducible voltammograms were obtained.

NPG was fabricated through the bottom-up DHBT potentiostatic electrodeposition method onto the pretreated AuE [30]. An optimized protocol was employed for the preparation of NPG/AuE, i.e., a constant potential of −4 V was applied for 50 s in the mixed solution of 50 mM $HAuCl_4$ and 4 M H_2SO_4. Afterwards, the obtained NPG/AuE-modified electrodes were washed with water and dried by nitrogen.

2.4. Construction of the Enzymatic Electrochemical Biosensor

The prepared NPG/AuE-modified electrode was incubated with 10 mM TA ethanol solution for 3 h, then rinsed with ethanol and distilled water successively to obtain a TA/NPG/AuE-modified electrode. After that, the obtained TA/NPG/AuE-modified electrode was activated in a mixed solution comprising 150 mM EDC and 50 mM NHS. GK and GPO were dispersed in 0.1 M PB (pH 7.0), respectively, and the final concentration of both was 6 U μL^{-1}. The isovolumic mixture of the GK and GPO solution was dispersed into a transparent CHIT solution (0.625 g of CHIT dissolved in 1 wt% acetic acid solution) in a volume ratio of 1:1. A total of 5 μL of the final mixture was dropped on the activated TA/NPG/AuE electrode, and the GK/GPO/CHIT/TA/NPG/AuE biosensor was constructed after drying at 4 °C overnight. For comparison, the GK/GPO/TA/NPG/AuE and GK/GPO/CHIT/NPG/AuE electrode were also prepared as above. These biosensors were stored in 0.1 M PB (pH 7.0) at 4 °C when not in use.

2.5. Application of Glycerol Biosensor in Real Samples

Red wine and white wine samples were purchased from a local supermarket, Guangzhou, China. Before detection was carried out, samples were diluted to the appropriate concentration in order to adjust the glycerol concentration in the wine to the dynamic concentration range of the sensors. Briefly, 100 μL of wine sample was mixed with PB (0.1 M, pH 7.0) at a volume ratio of 1:100. The GK/GPO/CHIT/TA/NPG/AuE biosensor was applied to detect the glycerol content of the above mixture, employing the standard addition method.

3. Results and Discussion

3.1. Structural and Morphological Characterization of the As-pPrepared NPG

For modification materials of the enzyme electrode, properties such as high specific surface area, high porosity, and controlled morphology are of vital importance. In the DHBT technique, the size and rate of the evolution of hydrogen bubbles can act as a dynamic template for the depositing metal atoms, thus forming porous material with a three-dimensional porous structure [31,32]. During the hydrogen bubble template electrodeposition process, H^+ is reduced to H_2, accompanied by the deposition of gold ions in the interstitial spaces of bubbles. The generated gold skeleton forces small bubbles to coalesce, resulting in the increase of its internal pore size layer by layer until these bubbles spontaneously escape from the surface and leave uniform porous material on the substrate electrode [31].

The microstructure and morphology of electrodeposited films can be adjusted conveniently by applying different deposition conditions, particularly deposition potential and deposition time. Cyclic voltammetry experiments were conducted in 1 M H_2SO_4 solution on the NPG/AuE-modified electrodes prepared at different potentials (−1, −2, −3 and −4 V) for 50 s, and at the potential of −4 V for various deposition times (10, 30, 50, 70 and 90 s), as well as bare AuE. The CV curves are shown in Figure 2. From Figure 2, it can be

found that two anodic peaks were observed at ca. 1.2 V and 1.4 V on all of the CV curves, which attributed to oxidation on gold ((200), (220), (311), and (111), respectively) [32]. The cathodic peak at ca. 0.9 V was associated with electrochemical reduction of gold oxide during the reverse scan and was proportional to the actual surface area of deposited materials. Figure 2a indicates that the reduction peaks of NPG/AuE-modified electrodes are significantly higher than bare AuE and increase with the negative shift of electrodeposited potential. This is because the overall surface of obtained NPG films is relatively compact due to the lower rate of H_2 evolution at lower overpotential (−1, −2, and −3 V), as shown in Figure S1a–c, while the one prepared at −4 V exhibits higher porosity that increases the surface area effectively and makes it suitable for enzyme immobilization (Figure S1d). From the voltammogram of Figure 2b, it can be seen that the extension of deposition time is particularly significant for the improvement of the reduction peak, which means that the surface area of NPG film continues to increase in the bottom-up growing process over time. Only an irregular coral-like structure deposited for 10 s (Figure S2a), macropores structure contour appeared after 30 s (Figure S2b), and an obvious uniform honeycomb-like NPG formed until 50 s (Figure S2c); then, the thicker films produced with increased time to 70 and 90 s (Figure S2d,e). However, it is worth noting that a thicker film is not more conducive to the performance of electrochemical sensors as the increase in noise level of measurements and possible structure collapse. Given these considerations, the selected electrodeposited potential and time for the preparation of NPG/Au-modified electrodes are −4 V and 50 s, respectively.

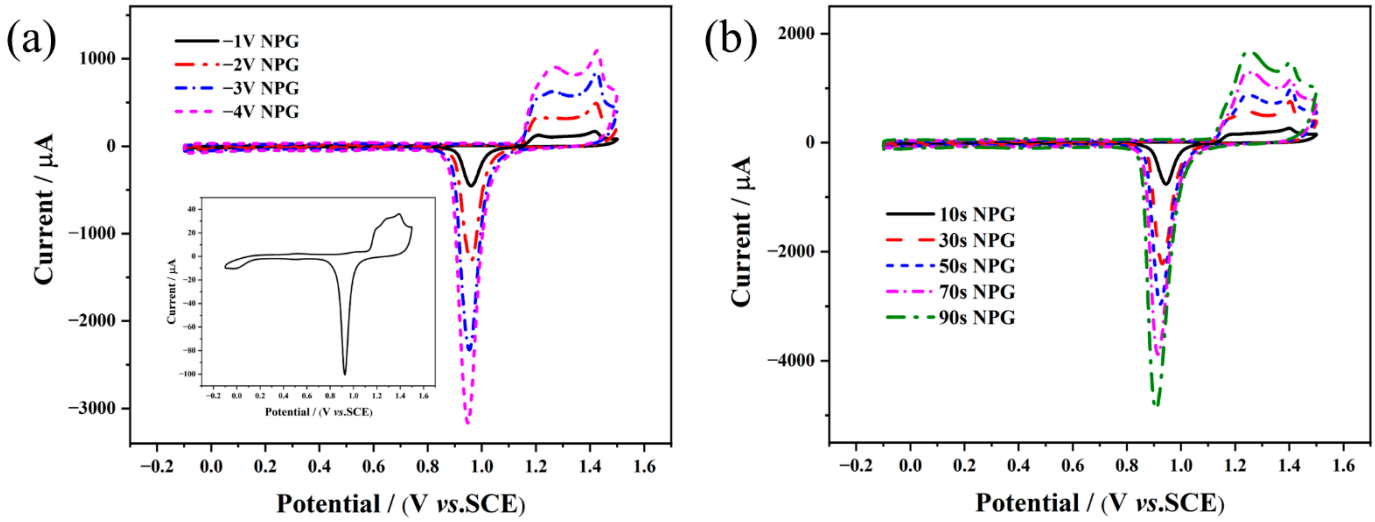

Figure 2. CVs of NPG/AuE-modified electrodes prepared (**a**) at different potentials (−1, −2, −3 and −4 V) for fixed time (50 s) and (**b**) at a fixed potential (−4 V) for different times (10, 30, 50, 70 and 90 s), and bare Au electrode (inset of (**a**)) recorded in 1 M H_2SO_4 solution at a scan rate of 100 mV s^{-1}.

The morphologies of prepared NPG which electrodeposited at −4 V for 50 s were characterized by SEM at different magnifications. As depicted in Figure 3a–c, the obtained film has a typical three-dimensional honeycomb structure with the increased pore size diameter toward the outer surface and gold skeleton composed of nano dendrites (Figure 3c), which is in line with the expectation of NPG prepared by DHBT. Furthermore, EDS compositional analysis, shown in Figure 3d, revealed that only Au was detected and proved the highly purity of NPG film prepared by the selected approach. The NPG prepared at optimal parameters was used to construct a glycerol enzymatic electrochemical biosensor in the following studies.

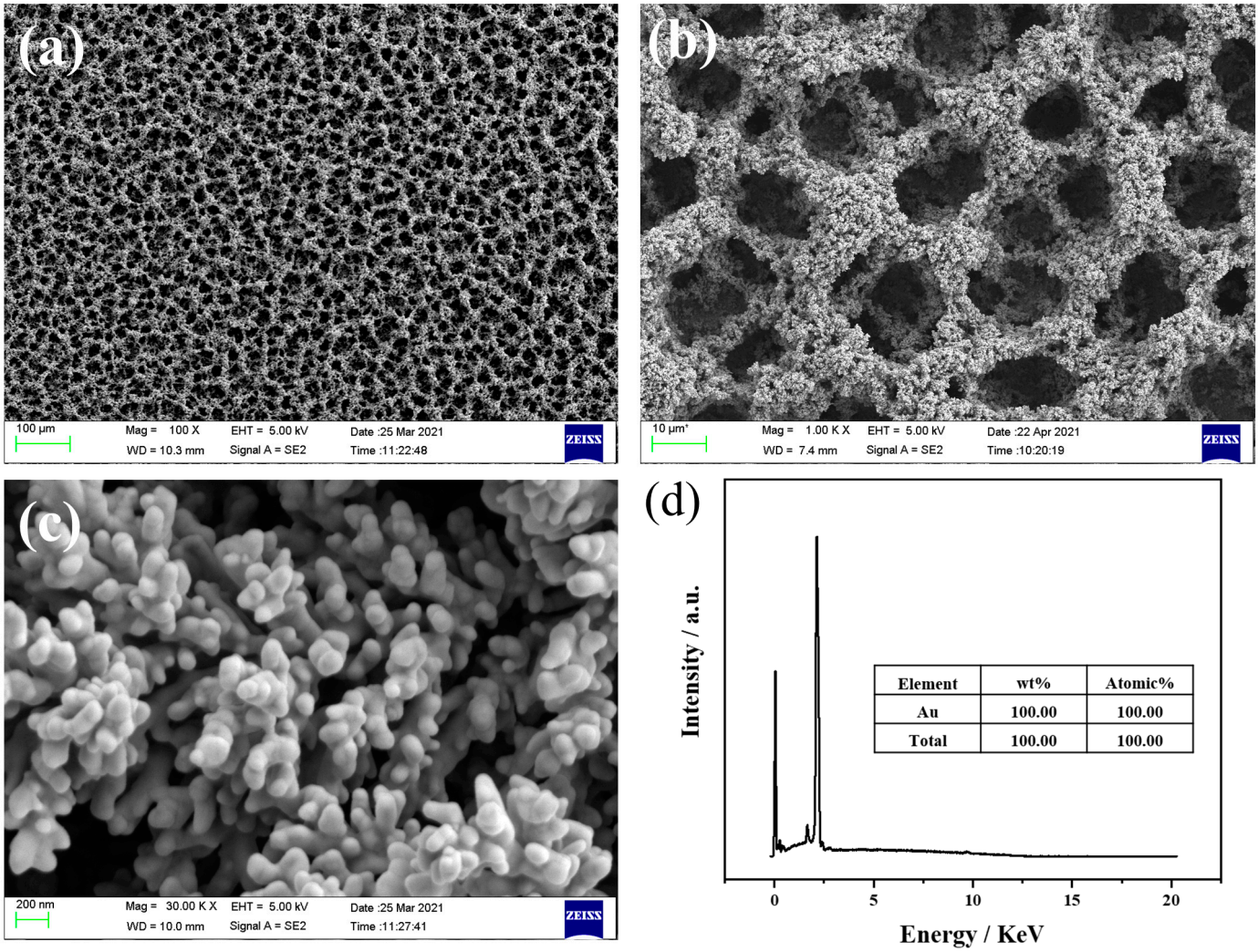

Figure 3. SEM images of NPG electrodeposited at −4 V for 50 s at (**a**) 100 times magnification, (**b**) 1000 times magnification, and (**c**) 30,000 times magnification, along with the corresponding EDS spectral (**d**).

3.2. Electrochemical Properties of Different Modified Electrodes

To demonstrate the successful preparation of the thioctic acid self-assembly membrane, CV experiments of the NPG/AuE-modified electrode before and after TA self-assembly were performed in 5 mM $[Fe(CN)_6]^{3-/4-}$ solution containing 0.1 M KCl. As could be seen in Figure 4a, the NPG/AuE-modified electrode shows a well-defined pair of redox peaks. After immersion, its peak current and double layer capacitance decrease obviously, which is attributed to the blocking of electron transfer by the decorated TA membrane, and the result indicates the successful preparation of a TA/NPG/AuE-modified electrode [27].

EIS measurements of different modified electrodes were performed to study the fabrication process of the biosensor. Figure 4b shows the obtained Nyquist plots of different modified electrodes. The semi-circle at higher frequencies corresponds to the electron transfer resistance (R_{ct}), which is related to the electron transfer kinetics for the redox probe on the surface of the electrode. The linear part at lower frequencies corresponds to the Warburg diffusion process [33]. The R_{ct} value for a bare AuE is 35.61 Ω, while the impedance of the NPG/AuE-modified electrode reduces prominently and exhibits an almost straight line. This change is attributed to the excellent conductivity of NPG. The R_{ct} value of the TA/NPG/AuE-modified electrode increases to 96.41 Ω due to the hindrance of the TA self-assembled membrane to the electron transfer on the electrode surface. Then, the R_{ct} values rise dramatically to 191.60 and 414.70 Ω for the CHIT/TA/NPG/AuE

and GK/GPO/CHIT/TA/NPG/AuE-modified electrodes, respectively, because the non-conductive chitosan and enzymes seriously hinder the electron transfer. As can be seen, the variation of impedance verified the successful construction of the biosensor.

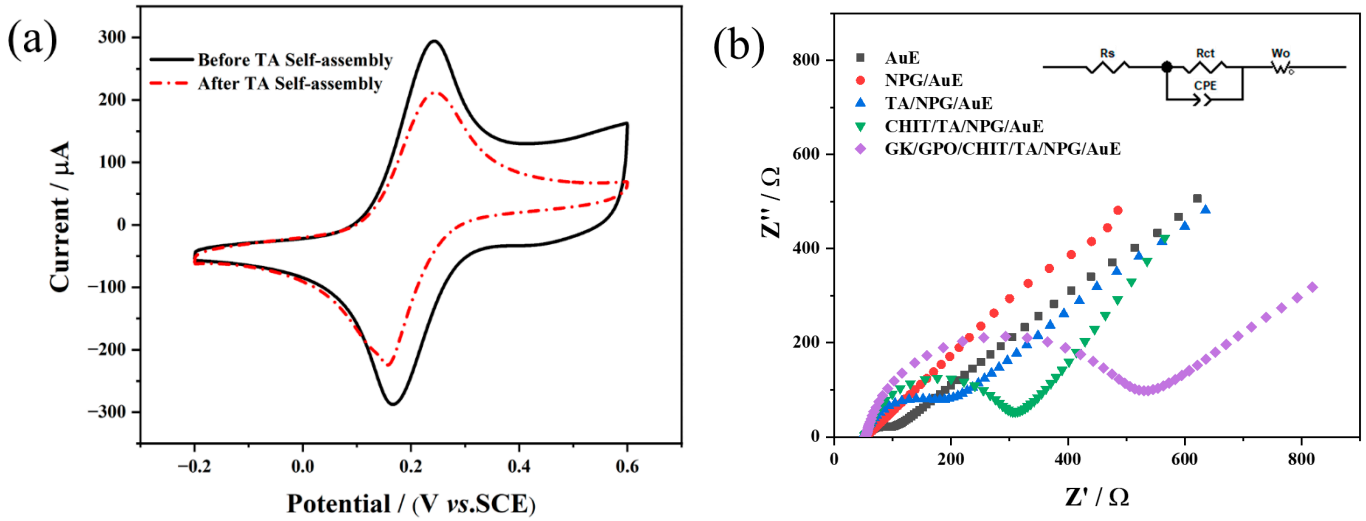

Figure 4. (**a**) CV curves of the NPG/AuE-modified electrode before and after TA self-assembly in 5 mM $[Fe(CN)6]^{3-/4-}$ solution containing 0.1 M KCl at a scan rate of 100 mV s^{-1} and (**b**) Nyquist plots of different modified electrodes in 5 mM $[Fe(CN)6]^{3-/4-}$ solution containing 0.1 M KCl.

3.3. Electrocatalytic Performance of the Fabricated Biosensor toward Glycerol

The electrocatalytic behaviors of different electrodes toward glycerol were evaluated by CV in 0.1 M PB (pH 7.0) containing 10 mM ATP, 2 mM Fm, 2 mM $MgCl_2$, and 10 mM glycerol. As displayed in Figure 5, only the typical reversible redox responses of the Fm/Fm^+ process appear at ca. 0.2 V for the AuE and NPG/AuE-modified electrode. In contrast, all the voltametric responses of the three enzyme-modified electrodes show an increase in the anodic peak current concomitant with a decrease in the cathodic peak current as a result of the cascade catalysis of glycerol by GK and GPO. The reaction mechanism can be explained by Equations (1)–(4). The anodic peak current of the GK/GPO/CHIT/TA/NPG/AuE-modified electrode is significantly higher than those of the GK/GPO/TA/NPG/AuE and GK/GPO/CHIT/NPG/AuE-modified electrodes. This certifies that combining covalent bonding and embedding methods to immobilize enzymes is beneficial to improve the catalytic performance of the enzymatic biosensor.

To further improve the sensing performance of the GK/GPO/CHIT/TA/NPG/AuE biosensor, several variables were optimized by CV in 0.1 M PB containing 10 mM glycerol at a scan rate of 50 mV s^{-1}. All experimental parameters remained constant except the research object during the optimization process. As shown in Figure S3a,b, the influence of TA self-assembled time and CHIT concentration on the enzyme immobilization effect was successively investigated. It was clear that the anodic peak current is the highest when TA self-assembled time and chitosan concentration are 3 h and 12.5 mg mL^{-1}, respectively. The loading amount of the enzyme has a great influence on the catalytic performance of the biosensor, so the GK/GPO concentration was optimized (Figure S3c). It can be seen that the peak current goes up gradually with the GK/GPO concentration increase and then remains steady beyond 6 U μL^{-1}, indicating that the load of GK/GPO reaches saturation when GK/GPO concentration increases to 6 U μL^{-1}. The concentration of ATP, Fm, and $MgCl_2$ can also affect the enzyme-catalyzed reaction rate and electron transfer efficiency of the biosensor. Subsequently, the amount of these additives in test solution were optimized from 5~25 mM for ATP, 2~10 mM for Fm, and 2~10 mM for $MgCl_2$. As displayed in Figure S3d–f, the highest biosensor response is obtained with 20 mM ATP, 8 mM Fm, and 8 mM $MgCl_2$, respectively. The solution pH can also be a key factor for the catalytic activity of the enzyme-modified electrode. Therefore, the effect of pH values was studied from

6.0 to 8.0 (Figure S3g). It can be seen that the maximum peak current appears at pH 7.0. This indicates that acidic or alkaline conditions are disadvantageous to the activity of GK and GPO.

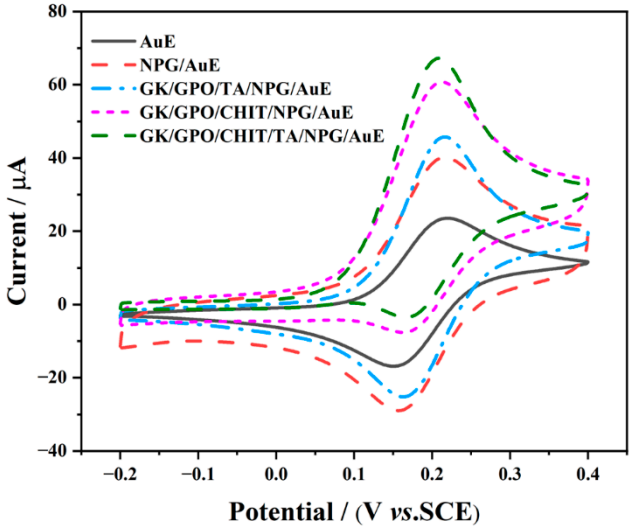

Figure 5. CV curves of the as-prepared modified electrodes in 0.1 M PB (pH 7.0) containing 10 mM ATP, 2 mM Fm, 2 mM $MgCl_2$, and 10 mM glycerol at a scan rate of 50 mV s^{-1}.

The influence of scan rate on the catalytic current was also investigated in the range of 25 to 200 mV s^{-1}. From Figure S4a, it can be seen that the anodic current increased with the increase of scan rates. The natural logarithm of the peak current (ln (I_p)) has a good linear relationship with the natural logarithm of the scan rate (ln (v)) (R^2 = 0.9966). As shown in Figure S4b, the slope value of 0.534 suggests that the catalytic reaction process of glycerol on the GK/GPO/CHIT/TA/NPG/AuE biosensor is diffusion-controlled [34].

3.4. Analytical Performance of the Fabricated Biosensor

The current response of the GK/GPO/CHIT/TA/NPG/AuE biosensor to glycerol was investigated under 0.1 M PB (pH 7.0) containing 20 mM ATP, 8 mM Fm, and 8 mM $MgCl_2$. As can be seen in Figure 6a, the anodic peak currents increase linearly with glycerol concentration increase, and there is a good linear relationship between the oxidation peak currents and glycerol concentration from 0.1 to 5 mM (Figure 6b). The linear regression equation is expressed as I(μA) = 9.173C (mM) + 71.421, with the coefficient of determination of R^2 = 0.9923, in which I and C are the response current and glycerol concentration, respectively. The sensitivity, calculated as the slope of the calibration curve, is 9.17 μA mM^{-1}. Based on the signal-to-noise ratio of 3, the low limit of determination was estimated to be 77.08 μM. It can be seen from Table 1 that the GK/GPO/CHIT/TA/NPG/AuE biosensor usually possesses a wider determination range and higher sensitivity.

Table 1. Electrochemical sensors for the determination of glycerol reported in literature.

Sensors	Sensitivity (μA mM^{-1})	Linear Range (mM)	LOD (μM)	References
GK/CK/CRE/HRP/GPE/AuE	0.80	0.005~0.64	1.96	[35]
ADH/TTF/CNT/GE	2.06 *	0.05~1	18	[36]
FeS/NAD^+/GIDH	0.025	1~25	160	[37]
GKNPs/GPONPs/GrONPs/PGE	8.59 *	0.001~60	0.002	[29]
AAM/NNMBA/AuNPs/Au-SPE	0.58	0.22~2.47	0.01	[38]
GK/GPO/CHIT/TA/NPG/AuE	9.17	0.1~5	77.08	This work

* Sensitivity value normalized by cm^2.

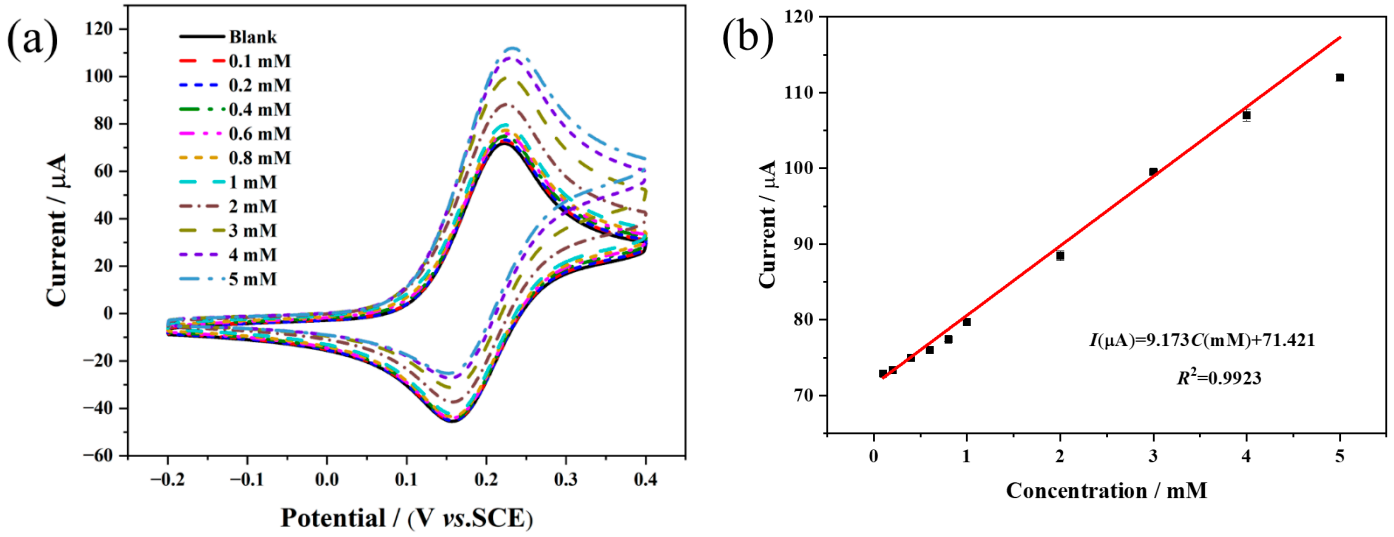

Figure 6. (**a**) Current response of GK/GPO/CHIT/TA/NPG/AuE biosensor to different concentrations of glycerol in 0.1 M PB (pH 7.0) containing 20 mM ATP, 8 mM Fm, and 8 mM $MgCl_2$ at a scan rate of 50 mV s^{-1} and (**b**) corresponding linear relationship between oxidation current and concentration of glycerol.

3.5. Selectivity, Repeatability, and Stability of the Fabricated Biosensor

The selectivity of the enzymatic electrochemical biosensor is an important characteristic for the specific recognition of the target substrate in real samples. According to the possible existence of interfering species in wine, the influence of 1 mM glucose (Glu), 1 mM urea, 1 mM citric acid (CA), 0.1 mM ascorbic acid (AA) and 5 mM ethanol (ET) on the response current of the GK/GPO/CHIT/TA/NPG/AuE biosensor were investigated in 0.1 M PB (pH 7.0) containing 20 mM ATP, 8 mM Fm, and 8 mM $MgCl_2$ and 1 mM glycerol (GLY). From Figure 7, it can be seen that the peak current variation caused by the above-mentioned interferents is less than 1%, indicating that the biosensor has satisfactory selectivity for glycerol.

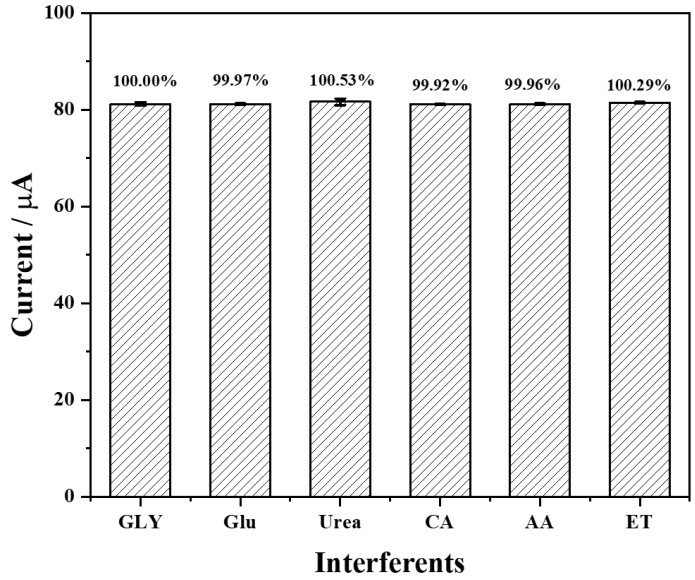

Figure 7. The effect of 1 mM Glu, 1 mM urea, 1 mM CA, 0.1 mM AA, and 5 mM ET on the response current of the as-prepared biosensor in 0.1 M PB (pH 7.0) containing 20 mM ATP, 8 mM Fm, 8 mM $MgCl_2$, and 1 mM glycerol at a scan rate of 50 mV s^{-1}.

The repeatability was also evaluated under the same conditions using five batches of the GK/GPO/CHIT/TA/NPG/AuE biosensor in 0.1 M PB (pH 7.0) containing 20 mM ATP, 8 mM Fm, 8 mM $MgCl_2$, and 1 mM glycerol. There is a low relative standard deviation (RSD) value of 2.48% (Figure S5), reflecting a good repeatability for the prepared biosensor.

Furthermore, the long-term stability of the GK/GPO/CHIT/TA/NPG/AuE biosensor was investigated by measuring the current response in 0.1 M PB (pH 7.0) containing 20 mM ATP, 8 mM Fm, 8 mM $MgCl_2$, and 1 mM glycerol. The response current of the as-prepared biosensor decreases 3.28% after 8 days (Figure S6), suggesting its great long-term stability. This may be attributed to the great biocompatibility of NPG, which can prevent the enzyme on the surface of the modified electrode from inactivation or falling off.

3.6. Application of the Biosensor in Actual Food Samples

To further test the performance of the GK/GPO/CHIT/TA/NPG/AuE biosensor in practical application, two dry wines (one red and one white) were purchased from the local supermarket and analyzed using the standard addition method. Taking into account the fact that the glycerol level in wines is far higher than the determination range of the biosensor, dilution of the samples was necessary. Then, glycerol standard solutions of two different concentrations (0.5 and 1 mM) were added into the diluted wine samples and measured by CV method. The results are showed in Table 2. It can be found from Table 2 that the original glycerol concentration in red wine is higher than that in white wine, which attributes to the higher fermentation temperature of the production process of wine [5]. The recoveries range is from 100.49% to 105.07% for the two samples, and RSD (n = 3) is lower than 4.14% for red wine and 3.33% for white wine. Thus, the as-prepared biosensor is reliable and can be applied for sensitive and rapid glycerol determination in actual food samples.

Table 2. Recovery for determination of glycerol in wines.

Samples	Original (mM)	Added (mM)	Detected (mM)	Recovery (%)	RSD (%)
Red wine	0.74	0.5	1.27	102.76	4.14
		1	1.75	101.03	1.65
White wine	0.41	0.5	0.96	105.07	2.06
		1	1.42	100.49	3.33

4. Conclusions

In summary, a novel glycerol biosensor based on chitosan- and thioctic-acid-modified nanoporous gold co-immobilization GK and GPO was successfully fabricated. The NPG prepared by DBHT had a porous microstructure, large specific surface area, and high conductivity. This work improved the catalytic performance and stability of enzyme-modified electrodes by chitosan embedding and thioctic-acid-modified nanoporous gold covalent bonding. The superior conductivity of NPG can enhance the electron transfer in the modified electrode, and the porous microstructure of NPG is beneficial to immobilize the GK and GPO, which can effectively protect the enzyme against inactivation and denaturation. The resulting GK/GPO/CHIT/TA/NPG/AuE biosensor exhibits a relatively wide linear range, high sensitivity, and low determination limit and great selectivity, repeatability, and stability. It can be applied for the determination of glycerol in real samples. Additionally, the biosensor holds great point-of-care application potential in environmental monitoring, public health, and food safety.

Supplementary Materials: The following supporting information can be downloaded at: https://www.mdpi.com/article/10.3390/chemosensors10070258/s1, Figure S1: SEM images of NPG electrodeposited at (a) −1, (b) −2, (c) −3 and (d) −4 V for 50 s; Figure S2: SEM images of NPG electrodeposited at −4 V for (a) 10, (b) 30, (c) 50, (d) 70 and (e) 90 s; Figure S3: Effect of several variables on the response current of the GK/GPO/CHIT/TA/NPG/AuE biosensor: (a) TA self-assembled time, (b) the concentration of CHIT, (c) the concentration of GK/GPO, (d) the concentration of ATP,

(e) the concentration of Fm, (f) the concentration of $MgCl_2$ and (g) pH; Figure S4: (a) CV response of the GK/GPO/CHIT/TA/NPG/AuE biosensor measured in 0.1 M PB (pH 7.0) containing 20 mM ATP, 8 mM Fm, 8 mM $MgCl_2$ and 1 mM glycerol at different scan rates (25~200 $mV \cdot s^{-1}$), and (b) corresponding linear relationship between anodic peak current and scan rate; Figure S5: Repeatability of the GK/GPO/CHIT/TA/NPG/AuE modified electrode in 0.1 M PB (pH 7.0) containing 20 mM ATP, 8 mM Fm, 8 mM $MgCl_2$ and 1 mM glycerol at a scan rate of 50 $mV \cdot s^{-1}$; Figure S6: Storage stability of the GK/GPO/CHIT/TA/NPG/AuE modified electrode in 0.1 M PB (pH 7.0) containing 20 mM ATP, 8 mM Fm, 8 mM $MgCl_2$ and 1 mM glycerol at a scan rate of 50 $mV \cdot s^{-1}$.

Author Contributions: Conceptualization, J.P.; methodology, C.Y.; validation, J.P., C.Y., and F.W.; formal analysis, J.P., K.J., and C.Y.; investigation, C.Y. and K.J.; resources, F.W.; data curation, C.Y., K.J., and X.L.; writing—original draft preparation, C.Y.; writing—review and editing, J.P. and F.W.; visualization, C.Y. and X.L.; supervision, J.P.; project administration, J.P.; funding acquisition, J.P. and F.W. All authors have read and agreed to the published version of the manuscript.

Funding: This work was funded by the National Natural Science Foundation of China (Nos. 21975079 and 21968031).

Data Availability Statement: Data are contained within the article or supplementary material.

Conflicts of Interest: The authors declare no conflict of interest.

References

1. Gamella, M.; Campuzano, S.; Reviejo, A.J.; Pingarrón, J.M. Integrated multienzyme electrochemical biosensors for the determination of glycerol in wines. *Anal. Chim. Acta* **2008**, *609*, 201–209. [CrossRef] [PubMed]
2. Gawel, R.; Sluyter, S.V.; Waters, E.J. The effects of ethanol and glycerol on the body and other sensory characteristics of Riesling wines. *Aust. J. Grape Wine Res.* **2007**, *13*, 38–45. [CrossRef]
3. Jones, P.R.; Gawel, R.; Francis, I.L.; Waters, E.J. The influence of interactions between major white wine components on the aroma, flavour and texture of model white wine. *Food Qual. Prefer.* **2008**, *19*, 596–607. [CrossRef]
4. Compagnone, D.; Esti, M.; Messia, M.C.; Peluso, E.; Palleschi, G. Development of a biosensor for monitoring of glycerol during alcoholic fermentation. *Biosens. Bioelectron.* **1998**, *13*, 875–880. [CrossRef]
5. Šehović, D.; Petravić, V.; Marić, V. Glycerol and wine industry clycerol determination in grape must and wine. *Kem. U Ind./J. Chem. Chem. Eng.* **2004**, *53*, 505–516.
6. Dias, A.N.; Cerqueira, M.B.R.; Moura, R.R.D.; Kurz, M.H.S.; Clementin, R.M.; D'oca, M.G.M.; Primel, E.G. Optimization of a method for the simultaneous determination of glycerides, free and total glycerol in biodiesel ethyl esters from castor oil using gas chromatography. *Fuel* **2012**, *94*, 178–183. [CrossRef]
7. De Almeida Cozendey, D.; De Oliveira Muniz, R.; Cavalcante Dos Santos, R.; Gimenes De Souza, C.; França De Andrade, D.; Antonio D'avila, L. Quantitative analysis of free glycerol in biodiesel using solid-phase extraction and high-performance liquid chromatography. *Microchem. J.* **2021**, *168*, 106347. [CrossRef]
8. Fernandes, E.N.; De Campos Moura, M.N.; Costa Lima, J.L.F.; Reis, B.F. Automatic flow procedure for the determination of glycerol in wine using enzymatic reaction and spectrophotometry. *Microchem. J.* **2004**, *77*, 107–112. [CrossRef]
9. Monošík, R.; Magdolen, P.; Streďanský, M.; Šturdík, E. Monitoring of monosaccharides, oligosaccharides, ethanol and glycerol during wort fermentation by biosensors, HPLC and spectrophotometry. *Food Chem.* **2013**, *138*, 220–226. [CrossRef]
10. Ghica, M.E.; Brett, C.M.A. Development and Applications of a Bienzymatic Amperometric Glycerol Biosensor Based on a Poly (Neutral Red) Modified Carbon Film Electrode. *Anal. Lett.* **2006**, *39*, 1527–1542. [CrossRef]
11. Pereira, D.F.; Santana, E.R.; Spinelli, A. Electrochemical paper-based analytical devices containing magnetite nanoparticles for the determination of vitamins B2 and B6. *Microchem. J.* **2022**, *179*, 107588. [CrossRef]
12. Narwal, V.; Pundir, C.S. Fabrication of glycerol biosensor based on co-immobilization of enzyme nanoparticles onto pencil graphite electrode. *Anal. Biochem.* **2018**, *555*, 94–103. [CrossRef] [PubMed]
13. Zhang, Y.; Li, Y.; Wu, W.; Jiang, Y.; Hu, B. Chitosan coated on the layers' glucose oxidase immobilized on cysteamine/Au electrode for use as glucose biosensor. *Biosens. Bioelectron.* **2014**, *60*, 271–276. [CrossRef]
14. Felipe, Q.J.A.; Javier, Q.B.; Diego, C.A.; Emilia, M. Metal free electrochemical glucose biosensor based on N-doped porous carbon material. *Electrochim. Acta* **2020**, *367*, 137434. [CrossRef]
15. Wu, L.; Gao, J.; Lu, X.; Huang, C.; Dhanjai; Chen, J. Graphdiyne: A new promising member of 2D all-carbon nanomaterial as robust electrochemical enzyme biosensor platform. *Carbon* **2020**, *156*, 568–575. [CrossRef]
16. Wonyong, J.; Hyughan, K.; Youngbong, C. Development of a Glucose Sensor Based on Glucose Dehydrogenase Using Polydopamine-Functionalized Nanotubes. *Membranes* **2021**, *11*, 384. [CrossRef]
17. Sethuraman, V.; Sridhar, T.; Sasikumar, R. Development of an electrochemical biosensor for determination of dopamine by gold modified poly (thiophene-3-boronic acid)-polyphenol oxidase modified electrode. *Mater. Lett.* **2021**, *302*, 130387. [CrossRef]

18. Sukeri, A.; Bertotti, M. Electrodeposited honeycomb-like dendritic porous gold surface: An efficient platform for enzyme-free hydrogen peroxide sensor at low overpotential. *J. Electroanal. Chem.* **2017**, *805*, 18–23. [CrossRef]
19. Zhang, Q.; Cheng, W.; Wu, D.; Yang, Y.; Feng, X.; Gao, C.; Meng, L.; Shen, X.; Zhang, Y.; Tang, X. An electrochemical method for determination of amaranth in drinks using functionalized graphene oxide/chitosan/ionic liquid nanocomposite supported nanoporous gold. *Food Chem.* **2022**, *367*, 130727. [CrossRef]
20. Yang, X.N.; Huang, X.B.; Hang, R.Q.; Zhang, X.Y.; Qin, L.; Tang, B. Improved catalytic performance of porcine pancreas lipase immobilized onto nanoporous gold via covalent coupling. *J. Mater. Sci.* **2016**, *51*, 6428–6435. [CrossRef]
21. Ng, A.K.; Welborn, S.S.; Detsi, E. Time-dependent power law function for the post-dealloying chemical coarsening of nanoporous gold derived using small-angle X-ray scattering. *Scr. Mater.* **2022**, *206*, 114215. [CrossRef]
22. Welborn, S.S.; Simafranca, A.; Wang, Z.; Wei, H.; Detsi, E. Chelation-mediated synthesis of nanoporous gold at near-neutral pH and room temperature by free corrosion dealloying of gold-copper alloy driven by oxygen reduction. *Scr. Mater.* **2021**, *200*, 113901. [CrossRef]
23. Mie, Y.; Takayama, H.; Hirano, Y. Facile control of surface crystallographic orientation of anodized nanoporous gold catalyst and its application for highly efficient hydrogen evolution reaction. *J. Catal.* **2020**, *389*, 476–482. [CrossRef]
24. Rebbecchi, T.A.; Chen, Y. Template-based fabrication of nanoporous metals. *J. Mater. Res.* **2018**, *33*, 2–15. [CrossRef]
25. Plowman, B.J.; O'mullane, A.P.; Selvakannan, P.R.; Bhargava, S.K. Honeycomb nanogold networks with highly active sites. *Chem. Commun.* **2010**, *46*, 9182–9184. [CrossRef]
26. Cherevko, S.; Chung, C.-H. Direct electrodeposition of nanoporous gold with controlled multimodal pore size distribution. *Electrochem. Commun.* **2011**, *13*, 16–19. [CrossRef]
27. Kolodziej, A.; Fernandez-Trillo, F.; Rodriguez, P. Determining the parameters governing the electrochemical stability of thiols and disulfides self-assembled monolayer on gold electrodes in physiological medium. *J. Electroanal. Chem.* **2018**, *819*, 51–57. [CrossRef]
28. Zhong, X.M.; Wang, F.; Piao, J.H.; Chen, Y.T. Fabrication and application of a novel electrochemical biosensor based on a mesoporous carbon sphere@UiO-66-NH2/Lac complex enzyme for tetracycline detection. *Analyst* **2021**, *146*, 2825–2833. [CrossRef]
29. Narwal, V.; Pundir, C.S. Development of glycerol biosensor based on co-immobilization of enzyme nanoparticles onto graphene oxide nanoparticles decorated pencil graphite electrode. *Int. J. Biol. Macromol.* **2019**, *127*, 57–65. [CrossRef]
30. He, F.; Qiao, Z.; Qin, X.; Chao, L.; Tan, Y.; Xie, Q.; Yao, S. Dynamic gas bubble template electrodeposition mechanisms and amperometric glucose sensing performance of three kinds of three-dimensional honeycomb-like porous nano-golds. *Sens. Actuators B Chem.* **2019**, *296*, 126679. [CrossRef]
31. Plowman, B.J.; Jones, L.A.; Bhargava, S.K. Building with bubbles: The formation of high surface area honeycomb-like films via hydrogen bubble templated electrodeposition. *Chem. Commun.* **2015**, *51*, 4331–4346. [CrossRef] [PubMed]
32. Kumar, A.; Furtado, V.L.; Gonçalves, J.M.; Bannitz-Fernandes, R.; Netto, L.E.S.; Araki, K.; Bertotti, M. Amperometric microsensor based on nanoporous gold for ascorbic acid detection in highly acidic biological extracts. *Anal. Chim. Acta* **2020**, *1095*, 61–70. [CrossRef] [PubMed]
33. Parra-Alfambra, A.M.; Casero, E.; Vázquez, L.; Quintana, C.; Del Pozo, M.; Petit-Domínguez, M.D. MoS2 nanosheets for improving analytical performance of lactate biosensors. *Sens. Actuators B Chem.* **2018**, *274*, 310–317. [CrossRef]
34. Kumar, A.; Gonçalves, J.M.; Sukeri, A.; Araki, K.; Bertotti, M. Correlating surface growth of nanoporous gold with electrodeposition parameters to optimize amperometric sensing of nitrite. *Sens. Actuators B Chem.* **2018**, *263*, 237–247. [CrossRef]
35. Monošík, R.; Ukropcová, D.; Streďanský, M.; Šturdík, E. Multienzymatic amperometric biosensor based on gold and nanocomposite planar electrodes for glycerol determination in wine. *Anal. Biochem.* **2012**, *421*, 256–261. [CrossRef] [PubMed]
36. Ramonas, E.; Ratautas, D.; Dagys, M.; Meškys, R.; Kulys, J. Highly sensitive amperometric biosensor based on alcohol dehydrogenase for determination of glycerol in human urine. *Talanta* **2019**, *200*, 333–339. [CrossRef] [PubMed]
37. Mahadevan, A.; Fernando, S. An improved glycerol biosensor with an Au-FeS-NAD-glycerol-dehydrogenase anode. *Biosens. Bioelectron.* **2017**, *92*, 417–424. [CrossRef]
38. Motia, S.; Bouchikhi, B.; Llobet, E.; El Bari, N. Synthesis and characterization of a highly sensitive and selective electrochemical sensor based on molecularly imprinted polymer with gold nanoparticles modified screen-printed electrode for glycerol determination in wastewater. *Talanta* **2020**, *216*, 120953. [CrossRef]